7450–7464 *Nucleic Acids Research, 2018, Vol. 46, No. 14* *Published online 9 July 2018*
doi: 10.1093/nar/gky614

Engineering orthogonal synthetic timer circuits based on extracytoplasmic function σ factors

Daniela Pinto[1,†], Stefano Vecchione[2,†], Hao Wu[2], Marco Mauri[2], Thorsten Mascher[1] and Georg Fritz[2,*]

[1]Institute of Microbiology, Technische Universität (TU) Dresden, 01062 Dresden, Germany and [2]LOEWE-Center for Synthetic Microbiology (SYNMIKRO), Philipps-Universität Marburg, 35032 Marburg, Germany

Received February 20, 2018; Revised June 08, 2018; Editorial Decision June 25, 2018; Accepted June 26, 2018

ABSTRACT

The rational design of synthetic regulatory circuits critically hinges on the availability of orthogonal and well-characterized building blocks. Here, we focus on extracytoplasmic function (ECF) σ factors, which are the largest group of alternative σ factors and hold extensive potential as synthetic orthogonal regulators. By assembling multiple ECF σ factors into regulatory cascades of varying length, we benchmark the scalability of the approach, showing that these 'autonomous timer circuits' feature a tuneable time delay between inducer addition and target gene activation. The implementation of similar timers in *Escherichia coli* and *Bacillus subtilis* shows strikingly convergent circuit behavior, which can be rationalized by a computational model. These findings not only reveal ECF σ factors as powerful building blocks for a rational, multi-layered circuit design, but also suggest that ECF σ factors are universally applicable as orthogonal regulators in a variety of bacterial species.

INTRODUCTION

Synthetic biology aims at applying engineering principles to biological systems. But inherent complexity of living cells severely hampers the identification of simple and universally applicable design rules. For instance, synthetic circuits frequently lose their functionality when placed in different genetic backgrounds, even within the same species (1,2), showing that the behavior of regulatory parts strongly depends on cellular context. On a molecular scale there are numerous reasons for such failures, many of which are related to incomplete knowledge on how synthetic circuit components interact with the host organism, as reviewed, e.g., in (3). In order to minimize such undesired cross-talk, in recent years orthogonal, that is, context-independent regulators were derived from natural systems, including dCas9 (4), small transcription-activating RNAs (5), translational riboswitches (6), orthogonal transcription factors (7), as well as extracytoplasmic function (ECF) σ factors (8). While these regulators have a great potential for synthetic biology, they now need to be applied and thoroughly characterized in the context of synthetic circuit design to identify their features, advantages and potential limitations. Such comprehensive knowledge will be a prerequisite to establish them as standard building blocks in the field that can complement the limited number of well-established transcription factors used in most synthetic genetic regulatory circuits built to date, such as LacI, AraC or TetR (9–11).

In this study, we focus on ECF σ factors as building blocks for synthetic circuit design. These alternative σ factors are subunits of the RNA polymerase and are found in almost all bacterial species (12). They regulate diverse processes and often respond to stress conditions. ECF σ factors share a characteristic protein domain architecture of only two of the four conserved regions of housekeeping σ factors, σ_2 and σ_4, which are sufficient for both promoter recognition and core RNA polymerase binding (Figure 1A). Today we know more than 90 phylogenetically distinct ECF subgroups (12–15), most of which recognize group-specific target promoters distinct from the housekeeping ones (Figure 1A and B). Their small and modular structure together with their ability to recognize distinct promoter sequences makes ECF σ factors ideal building blocks for developing multiple, orthogonal switches that can be simultaneously used in a heterologous host. Indeed, Rhodius *et al.* identified about 20 highly orthogonal heterologous ECF σ factors in *Escherichia coli* that specifically activated their target promoters – with little cross-activation of other native or heterologous ECF target promoters (8). Despite these potential advantages for synthetic biology, ECF σ factors have rarely been used to construct insulated switches (16) or more complex circuits (17) *in vivo,* but, to our knowledge, no synthetic regulatory circuit comprising more than a single ECF σ factor has been constructed before. Hence, although the large diversity (12) and orthogonality between ECF sub-

*To whom correspondence should be addressed. Tel: +49 6421 28 22582; Fax: +49 6421 28 24430; Email: georg.fritz@synmikro.uni-marburg.de
†The authors wish it to be known that, in their opinion, the first two authors should be regarded as joint First Authors.

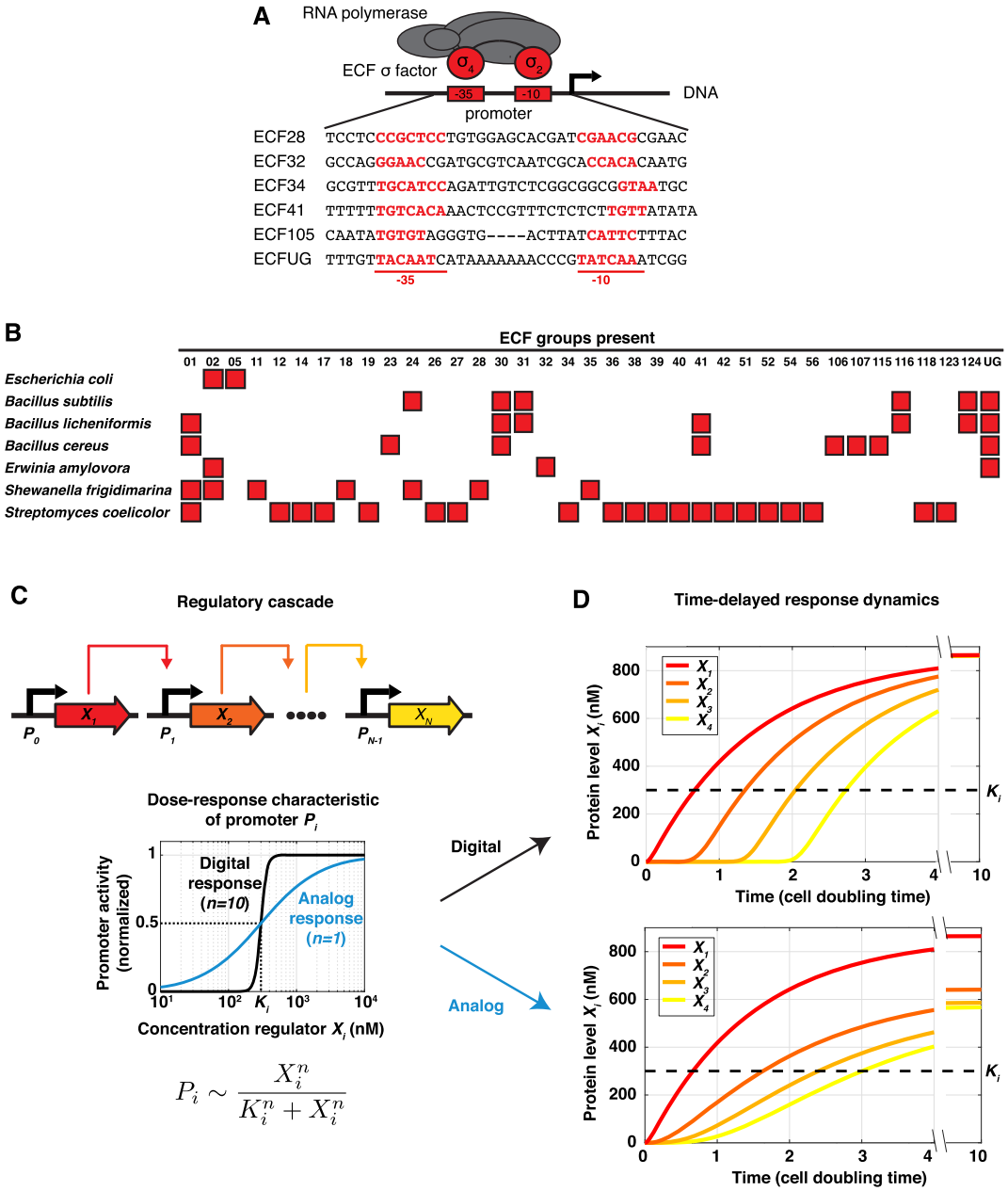

$$P_i \sim \frac{X_i^n}{K_i^n + X_i^n}$$

Figure 1. Extracytoplasmic function (ECF) σ factors as orthogonal building blocks for synthetic circuit design. (**A**) The σ_2 and σ_4 protein domains of ECF σ factors contact the −10 and −35 promoter regions, respectively, and thereby recruit RNA polymerase to specific target promoters (for a review see (56)) as shown in the lower part of the panel for the ECF σ factors used in this study. Note that the highlighted −35 and −10 sequences are putative promoter elements and have not been experimentally verified in all cases. Also note that sequence of the ECF28 and ECF34 promoters are modified variants of the ECF group 19 and group 18 promoters, as described in (8). (**B**) ECF σ factor groups found in *E. coli*, *B. subtilis* and the four species serving as donors of the ECFs used here, i.e., *Bacillus licheniformis* (ECF41 and ECFUG), *Bacillus cereus* (ECF105), *Erwinia amylovora* (ECF32), *Shewanella frigidimarina* (ECF28) and *Streptomyces coelicolor* (ECF34). (**C**) The temporal dynamics of gene regulatory cascades, in which a series of N regulators X_i sequentially activate the expression of a downstream regulator X_{i+1}, critically hinges on the quantitative dose–response characteristics of the involved promoters P_i. For promoters regulated in a highly cooperative manner (e.g. for a Hill coefficient $n = 10$, *black curve*), the transcriptional activity displays an almost digital increase as soon as the concentration of the cognate regulator exceeds the activation threshold K_i. In contrast, non-cooperatively regulated promoters (Hill coefficient $n = 1$, *blue curve*) feature an analog increase of transcriptional activity with increasing regulator concentration. (**D**) Time-delayed response dynamics in a cascade of digital (*top panel*) and analog (*bottom panel*) regulatory switches. For further details, refer to the main text.

groups suggests that multiple ECFs can be combined in a single cell, the scalability of the approach has never been studied. Moreover, it is currently unclear whether ECF σ factors can be used as orthogonal building blocks in organisms other than *E. coli*.

Here, we explore the potential of ECF σ factors as orthogonal building blocks for synthetic circuit design in two of the most widely used and phylogenetically distant model bacteria – *E. coli* and *Bacillus subtilis*. In both organisms we implemented increasingly complex ECF σ factor circuits, and thereby systematically probed the scalability of this approach. Our results demonstrate the successful construction of ECF σ factor cascades featuring the functionality of 'genetic timers' – circuits that activate a series of ECF σ factor genes with characteristic time delays. With the help of a quantitative mathematical model we rationalized the *in vivo* expression dynamics of a variety of timer circuits in *E. coli* and *B. subtilis*, showing that ECF σ factors display orthogonality even in multi-layered regulatory circuits. However, we also find that signal propagation within these cascades critically hinges on precise fine-tuning of input- and output-dynamic ranges, as theoretically predicted for non-cooperative regulatory cascades without feedback (18). These results unveil some of the fundamental strengths and limitations of ECF σ factors for synthetic circuit construction, suggesting that they are useful components for future work in synthetic biology. Taken together, this work broadens our understanding of ECF σ factors and provides insight into key design rules for synthetic ECF σ factor circuits in two phylogenetically diverse model bacteria.

MATERIALS AND METHODS

Plasmid assembly & strain development

All circuits for *E. coli* were assembled using the Modular Cloning (MoClo) system (19), which relies on Golden Gate cloning with type IIs endonucleases, the recognition sites of which are distal from their cut sites and thereby enable the directed assembly of multiple DNA parts in a simultaneous restriction/ligation reaction. Within the MoClo system multi-gene constructs can be assembled from libraries of defined genetic parts by using four sets of cloning vectors (Level 0, 1, M and P), which can be utilized in successive assembly steps. Different genetic parts (e.g. promoters, ribosome binding sequence, random DNA sequences, coding sequences and terminators) were PCR amplified and cloned in MoClo level 0 vectors, generating a library of level 0 modules (Supplementary Table S2.1). These modules were used to assemble different transcription units (TU) in MoClo Level 1 destination vectors (Supplementary Table S2.2). Finally multiple transcription units were joined to generate timer circuits in the medium copy number reporter plasmids pICH82094 (MoClo level P), its derivative pSVM-mc (MoClo Level M) or in plasmid pSV004 for chromosomal integration, as described below (see Supplementary Table S2). pSVM-mc was created by Gibson assembly using the primers GF078-GF089-GF080-GF081 to amplify the plasmid backbone from pICH82094, including the resistance cassette and the medium copy number origin of replication, and exchanging the MoClo fusion sites from level P to level M. The circuits assembled on these medium copy number plasmids were transformed in the *E. coli* reporter strain SV01. SV01 is a derivative of *E. coli* strain MK01 (20), in which we removed the chloramphenicol cassette by expression of the Cre recombinase (21). MoClo reactions were set up by pipetting in one tube 15 fmol of each DNA part (PCR product or plasmid), 1 μl of the required restriction enzyme (BsaI or BpiI), 1 μl of T4 DNA ligase (5 U/μl) and 2 μl of Thermo ligase buffer (10x) in a final reaction volume of 20 μl. The reaction was incubated in a thermocycler for 5 h at 37°C, 10 min at 50°C and 10 min at 80°C. 2 μl of the reaction mix were then added to 50 μl chemically competent DH5α cells, incubated for 30 min on ice and transformed by heat shock. 950 μl of liquid LB was then added to the transformation, and the cells were let to recover 45 min at 37°C. 40 μl of the transformation were plated on selective LB plates and then the colonies were tested by colony PCR and restriction digestion. All level 0 plasmids created as well as the final timer circuits were verified by sequencing.

Chromosomal integration of timer circuits in *E. coli* was achieved by site-specific recombination at HK022 phage attachment site using the conditional-replication, integration, and modular (CRIM) plasmids (22). Using LCR assembly we adapted the plasmid pAH68 (22) to the MoClo standard by adding the fusion sites of the vector pAGM8031 and exchanging the resistance cassette from ampicillin to chloramphenicol, generating the plasmid pSV004. This plasmid was used as destination vector to assemble 1- and 2-step timers using the MoClo cloning protocol. Subsequently, chromosomal integration was performed as described previously (22). Briefly 2 μl of the MoClo reaction were added to 50 μl chemically competent SV01 cells, carrying the CRIM helper plasmid pAH69, incubated for 30 min on ice and transformed by heat shock. 950 μl of liquid LB was then added to the transformation, and the cells were incubated at 37°C for 1 h and at 42°C for 30 min. 40 μl of the transformation were spread onto selective agar plates and incubated at 37°C. Colonies were tested by colony PCR using the primers P1–P2–P3–P4 (22), purified once non-selectively and then tested for antibiotic resistance for stable integration and loss of the helper plasmid.

All circuits for *B. subtilis* were created using general cloning procedures and all plasmids are BioBrick RFC10 compatible except for pDP3Clux07. The relevant parts were generated by PCR (see Supplementary Table S3) and purified using HiYield PCR Gel Extraction/PCR Clean-up kit (Süd-Laborbedarf GmbH, Gauting, Germany). Restriction reactions of EcoRI, XbaI, SpeI and PstI as well as ligation reactions were performed using enzymes and buffers from New England Biolabs (NEB; Ipswich, MA, USA) accordingly to the supplier's protocol. Plasmids were isolated using HiYield Plasmid Mini-kit (Süd-Laborbedarf GmbH, Gauting, Germany) and confirmed by sequencing. The constructed plasmids (Supplementary Table S3) were introduced into *B. subtilis* 168 strain as previously described (23). Integration of the plasmids into the chromosome was confirmed by colony PCR. Integration of pBS1K derivatives was confirmed by the inability to degrade starch while integration of pBS4S derivatives was confirmed through threonine autotrophy. A complete list of *E. coli* and *B. subtilis*

strains can be found in Supplementary Tables S2 and S3, respectively.

Microplate reader assays

Microplate reader assays in *E. coli* were performed as follows. For each strain a single bacterial colony was picked from selective plates and grown in liquid LB medium until stationary phase (37°C shaking at 250 rpm; 7-8 hours). The day-cultures were diluted 1:6000 into MOPS minimal medium (TEKNOVA Cat.No. M2106; 0.5% glycerol as carbon source) supplemented with appropriate antibiotics and grown over night (37°C shaking at 250 rpm) until they reached an optical density at 600 nm (OD_{600}) of 0.5–0.6. The cultures were then diluted to an OD_{600} of 0.05 in fresh MOPS minimal medium (see above, but without antibiotic selection) and 100 μl of culture were loaded in the wells of a black 96-well plate (GREINER catalog no.: 655097). Using a Tecan Infinite F200 pro microplate reader the plate was incubated for 7 h (37°C with shaking) and OD_{600} as well as luminescence were measured every 5 min. For switching cascades from the OFF to the ON state, after two hours of incubation cells were induced with indicated final concentrations of arabinose and incubation was resumed. For switching cascades from the ON to the OFF state, day-cultures were grown in the same medium as above, but supplemented with 10^{-4}% arabinose, until they reached an OD_{600} of 0.5–0.6. Cultures were then washed, diluted to an OD_{600} of 0.05 in fresh arabinose-free MOPS minimal medium, and incubated in a microplate reader as described above.

Microplate reader assays in *B. subtilis* were performed as previously described (24). Briefly, for each strain a single bacterial colony was picked from selective plates and grown overnight in liquid LB medium supplemented with the appropriate antibiotics (30°C with shaking). The cultures were then diluted 1:500 in fresh LB medium and incubated for 4 hours (30°C with shaking) until they reached an OD_{600} between 0.2 and 0.5, at which point they were diluted to an OD_{600} of 0.05 in pre-warmed LB and transferred to a 96-well plate. Using a BioTek Synergy™2 multimode microplate reader, the plate was incubated (30°C with shaking), measuring OD_{600} and luminescence every 5 min for 3 h. For switching cascades from the OFF to the ON state, cells were induced after 1 h, from the beginning of the measurement, with indicated final concentrations of bacitracin. For switching cascades from the ON to the OFF state, cells were induced with 10 μg/ml bacitracin for 1.5 h, then washed and re-suspended in fresh, pre-warmed LB medium without bacitracin and then incubated for additional 4 h.

Determination of ECF profiles

The complete set of protein sequences in FASTA format was downloaded from UniProt (25) for the following organisms: *Bacillus cereus* strain DSM 31, *Bacillus licheniformis* strain DSM 13, *Bacillus subtilis* strain 168, *Erwinia amylovora* strain CFBP1430, *Escherichia coli* strain K12, *Shewanella frigidimarina* strain NCIMB 400. The proteomes were then submitted to ECFfinder (12) for ECF identification and classification.

Computational model

The computational model developed in this study is detailed in the Supplementary Model Information.

Quantification and statistical analysis

Figures 2, 4, 5 and 6 all utilize statistical analysis, specifically the error bars around mean traces are computed as the standard deviation of experimental replicates. In all such plots, an experimental replicate refers to a separate experiment quantitated and executed in batch mode, using identical experimental parameters. The luciferase activity for each replicate in Figures 2, 4 and 5 was determined as follows. First, the raw luminescence data obtained from microplate reader measurements was background-corrected by subtracting luminescence values obtained from a control well containing the growth medium alone. Then we corrected for luminescence bleed-through (i.e. light-scattering) from neighbouring wells on the microplate, by using a de-convolution algorithm that will be published elsewhere (Mauri, Vecchione and Fritz, unpublished). Last, the resulting values were divided by the (background-corrected) optical density at each time point during the course of the experiment, which yields the luciferase activity in relative luminescence units per OD_{600} (RLU/OD). The time delay in gene induction was defined as the difference between the time at which the luciferase activity first exceeded its average pre-induction value by 2-fold, and the time point of inducer addition.

RESULTS

Gene regulatory cascades as biological timer circuits

To explore the potential of ECF σ factors for synthetic circuit design, we aimed at building gene regulatory cascades of varying length (Figure 1C), where an inducible promoter P_0 drives the expression of the first regulator X_1, which then activates expression of the downstream regulator X_2, etc., until the final target gene is activated. Such cascades serve as ideal test-bed to study whether multiple ECF σ factors indeed function as orthogonal regulators, and whether their quantitative characteristics are amenable to combining them into larger circuits. On a theoretical basis, it is well established that the dynamical response of such cascades can display a time delay between the inductions of individual genes (see e.g. (26)). For instance, let us assume the simple case in which all promoters in the cascade P_i ($i = 1, \ldots, N$) display a digital response characteristic, for which the activity sharply switches from OFF to ON if the concentration of the regulator X_i exceeds a threshold value K_i, as observed for cooperatively regulated promoters (Figure 1C, black curve). Upon induction of the first promoter, each regulator X_i in the cascade will then take a finite time to accumulate from its basal value to the threshold K_i required for inducing the expression of the downstream regulator (Figure 1D, top panel). This specific time delay depends on various parameters, such as protein production and decay rates or the activation thresholds K_i of each regulator. Interestingly, for these digital switches the overall time delay of the cascade scales linearly with the number of regulators included (Figure 1D, top panel), much like for timers

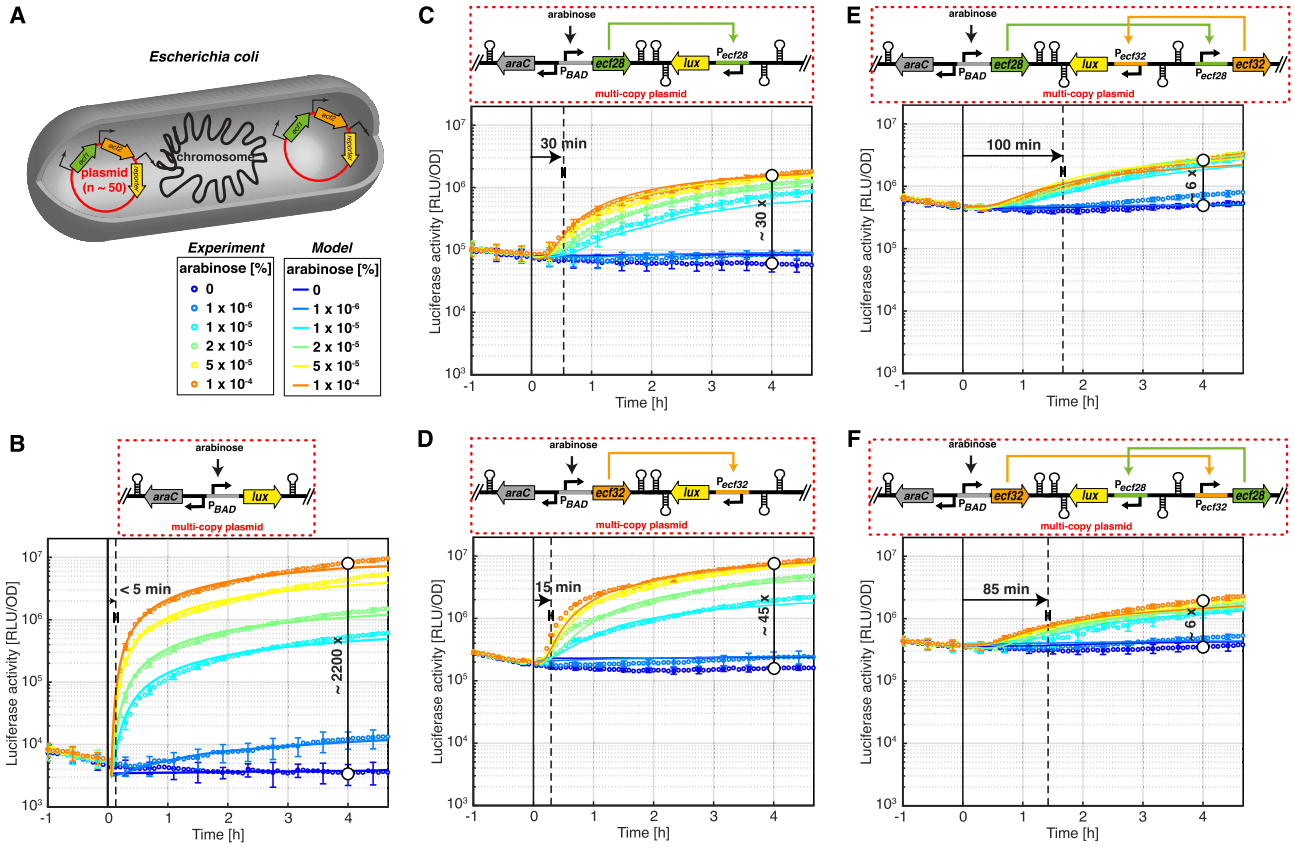

Figure 2. Time delayed response of synthetic ECF cascades in *E. coli*. (**A**) All circuits shown in the cartoons of (B–F) were introduced in *E. coli* strain SV01 on medium copy plasmid pSVM-mc (Supplementary Table S2). Panels (B–F) show the dynamical response of luciferase activity (shown in relative luminescence units normalized by the optical density measured at 600 nm) in synthetic ECF cascades featuring no (B), one (C, D) and two (E, F) ECF σ factors, after the addition of various concentrations of arabinose at t = 0 h (*black solid line*). The time delay of gene induction (*black dashed line*) is indicated for the highest arabinose concentration (10^{-4}%) and was defined as the time when luciferase activity first exceeded the pre-induction value by 2-fold. Maximal fold induction is also indicated. The experimental response dynamics (*circles*) was recorded during exponential growth, as described in Materials and Methods. The response dynamics of the computational model (*solid colored lines*) was obtained by a simultaneous fit of all experimental data in (B–F), showing that the behavior of all five circuits can be explained with one self-consistent set of physiological parameters (see Supplementary Table S3). Here time delays in the computational model (as given for 10^{-4}% arabinose) are: (**B**) 5 min, (**C**) 32 min, (**D**) 22 min, (**E**) 83 min and (**F**) 96 min.

in digital electronics, where the serial connection of multiple timers additively contributes to the time delay of the composite circuit.

Many biological switches, however, feature analog responses, for which the promoter activity increases gradually with increasing regulator concentrations (Figure 1C, blue curve). For instance, alternative σ factors bind RNA polymerase as monomers, leading to non-cooperative regulation of target promoters with low kinetic order (i.e. a Hill coefficient $n = 1$) (27). When combining multiple analog switches into a regulatory cascade, we thus expect that upon induction, rising regulator levels will cause a more gradual activation of target promoters, which may result in a temporal blur in the switching kinetics of individual stages in the cascade (Figure 1D, bottom panel). However, similar to the digital timers above also the cascade of analog switches is predicted to display an increasing overall time delay with increasing cascade length, suggesting that such cascades can still perform the function of a biological timer (Figure 1D, bottom panel). Closer inspection shows that in this case the time delay is no longer additive. Within our simple model this is caused by a decrease of the maximal protein levels from tier to tier, thereby reaching the activation thresholds only at later times. While the extent of signal loss may again sensitively depend on parameter values, such as protein expression and decay rates of individual regulators in the cascade, signal de-amplification is a general feature of non-cooperative regulatory cascades, as has been predicted theoretically for enzyme cascades with simple Michealis-Menten kinetics (18,28) and will be analyzed in greater detail further below. However, first we wondered whether ECF σ factor cascades would in fact show these hallmark features of analog regulatory cascades in an experimental setup.

Performance evaluation of ECF switches in a new *E. coli* setup

For the experimental implementation of ECF switches and cascades, we then established a genetic system to assemble circuits from a library of DNA parts in a rapid and scalable way. To this end we leveraged the modular cloning (MoClo) system (19), a Golden Gate-based vector system allowing for the hierarchical and modular assembly of transcription units into higher order circuits. Briefly, we gen-

erated a library of genetic parts (e.g. promoters, ribosome binding sites, coding sequences and terminators) in MoClo level 0 vectors, assembled them into transcription units (TUs) using MoClo level 1 vectors, which were finally combined into regulatory circuits in MoClo level M vectors (see Materials and Methods for details). To quickly test *in vivo* circuit performance, we created a new MoClo level M vector pSVM-mc that directly serves as medium copy number expression plasmid in *E. coli*. The integration of all parts on one plasmid has the advantage of maintaining the stoichiometry between the copy number of all circuit components at any time. In order to insulate transcription units (TUs) against transcriptional read-through or other polar effects (29), we placed neighbouring TUs in alternating orientations and introduced multiple terminators (30) as well as stretches of random, non-coding DNA between them, thereby abolishing any undesired cross-activation between neighbouring TUs (Supplementary Figure S1).

Next, we focussed on the 10 ECF σ factors that previously showed the most desirable characteristics for implementation in higher order circuits, *i.e.*, high activity, low cross-talk and little toxicity in *E. coli* strain DH10ß (8) (Supplementary Table S1). To assess the function of these ECF σ factors in our setup, we placed the ECF coding genes under the control of the arabinose-inducible P_{BAD} promoter and fused the ECF target promoters to a luciferase cassette from *Photorhabdus luminescens* (31), which has proven to be a highly sensitive reporter system for *in vivo* gene expression analyses (32). *E. coli* strain SV01, which constitutively expresses the arabinose permease *araE* and carries a deletion of the *araBAD* operon responsible for arabinose catabolism, was used to allow for a graded, arabinose-dependent induction of P_{BAD}(33) (see Materials and Methods and Supplementary Table S2). Finally, the functionality of the ECF σ factors was benchmarked by growing strain SV01 carrying plasmid-encoded ECF switches in defined minimal media (doubling time ∼150 min) and assaying luciferase activity for 4 h after the addition of arabinose. Overall, we found that all 10 ECF σ factors strongly activated their cognate target promoters (∼1000- to 10 000-fold over empty vector control) while displaying little toxicity (see Supplementary Figure S2). This result demonstrates that our setup allows for highly sensitive monitoring of ECF target promoter activity. Among all ECF σ factors tested, ECF28, ECF32 and ECF34 displayed the highest fold-induction of the target promoter (between 20 and 100-fold) and had no detectable deleterious effects on cell growth (Supplementary Figure S2), leading us to proceed with those ECF σ factors for further analysis.

Dynamical response of ECF switches and cascades in *E. coli*

Thereafter, we studied the timing behaviour in the induction of ECF28, ECF32 and ECF34 switches. Toward this end, we measured the kinetic response in luciferase activity after the induction of strains carrying the different ECF switches with various arabinose concentrations (Figure 2). In order to compare circuit dynamics between various ECF switches, we defined their response time as the time between the addition of the highest inducer concentration and the time at which luciferase activity first exceeds its pre-induction activity more than 2-fold. While the control strain harboring a P_{BAD}-*lux* construct showed a rapid response time of 5 min (Figure 2B), the activation of the ECF28, ECF32 and ECF34 switches was delayed by 15–30 min (Figure 2C, D and Supplementary Figure S3C). This suggests that the ECF target promoter activity relies on the gradual accumulation of functional ECF proteins, which generates a time delay between inducer addition (up-regulation of *ecf* expression) and target promoter activation. In contrast, we did not observe a significant increase of luciferase activity in any of the negative control circuits, which either lack the ECF σ factor or the ECF target promoter (Supplementary Figure S3), showing that the delayed response is specific to the slow accumulation of ECF σ factors. Based on the observed time delay and the fact that each circuit involves the expression of one *ecf* gene, we refer to them as 1-step timer circuits from now on.

Strikingly, when combining ECF32 and ECF28 into 2-step timer cascades in different permutations (Figure 2E and F), we found that the activation of the luciferase cassette by the second ECF in the cascade occurred with significantly longer delays of 100 min (Figure 2E) and 85 min (Figure 2F). This confirms our qualitative expectation that the time-delayed response that scales with the length of the ECF σ factor cascade (Figure 1C). Interestingly, the variability between time delays observed in independent biological replicates was less than 5 min (Figure 2; horizontal error bars). While such a characteristic time delay on population average does not necessarily imply a homogeneous timing in all cells of the culture, it clearly suggests robust circuit performance at the bulk level. Despite reproducible timing, however, we also noted that the 1-step and 2-step timer circuits displayed a reduced output-dynamic range when compared to the P_{BAD}-*lux* control strain (which we refer to as 0-step timer): while P_{BAD}-*lux* showed a 2200-fold induction upon arabinose addition, this reduces to a 30-fold and 45-fold induction in the ECF28 and ECF32 1-step timers (Figure 2C and D), respectively, down to a 6-fold induction in both 2-step timers (Figure 2E and F). Here, the decreasing dynamic range is largely caused by an increased baseline activity of the 1-step and 2-step timers even in the absence of arabinose. Note that the negative control strains, not expressing the second ECF in the 2-step timer cascade, also displayed non-cognate target promoter activity, although about 1000-fold weaker than the regulation by the cognate ECF (Supplementary Figure S4), indicating that the increasing baseline activity in the 2-step timers is caused by the cognate ECF σ factor and not the other ECF σ factor of the cascade. Interestingly, when combining all ECF σ factors into 3-step timer cascades (containing ECF28, ECF32 and ECF34 in two different permutations) the baseline increased even more, leading to an almost complete loss of their output-dynamic range (Supplementary Figure S5).

Computational model for ECF σ factor cascades

We developed a set of detailed computational models for the ECF timer circuits to test whether these experimental data can be rationalized at a quantitative level. In particular, we asked whether the dynamics and fold-change of the 2-step

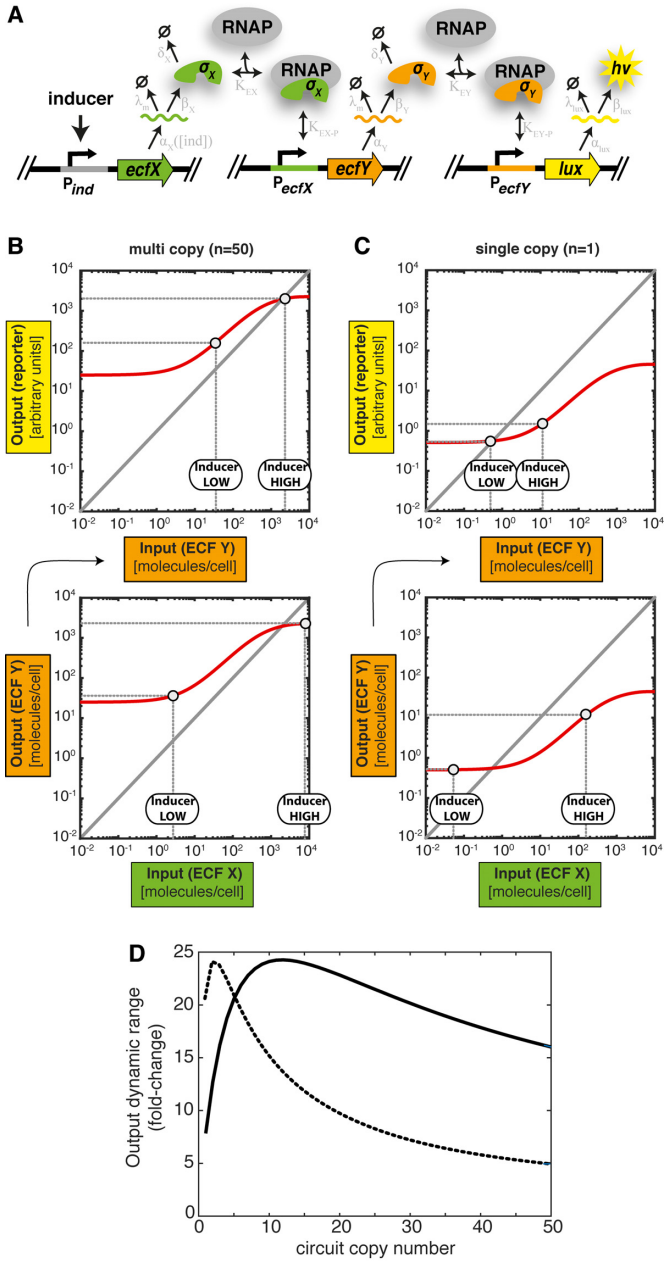

Figure 3. Computational model for ECF cascades. (**A**) Computational model for a σ factor cascade comprising two ECFs *X* and *Y*, the latter of which drives expression of the luciferase (*lux*) cassette. In the model we included transcription and translation of genes and mRNAs of *ecfX*, *ecfY* and the *lux* cassette, with transcription rates α_i and translation rates β_i ($i = X, Y, lux$). In addition, degradation and/or dilution of mRNA and protein species occur at rates λ_i and δ_i, respectively, ECF σ factors bind to core RNA polymerase with equilibrium dissociation constant K_{Ei} and the resulting holoenzymes bind to their cognate promoters with dissociation constant $K_{Ei\text{-}P}$ ($i = X, Y$). For further details please refer to the Supplemental Information. (**B**, **C**) Signal propagation in the 2-step timer cascade for plasmid-borne (B; copy number $n = 50$) and for chromosomal circuit expression (C; copy number $n = 1$). The lower panel shows the equilibrium abundance of ECF Y proteins (output of the first ECF promoter P_{ecfX}) as a function of the abundance of ECF X proteins (all units are molecules/cell). Accordingly, on top, the equilibrium abundance of reporter proteins (output of the second ECF promoter P_{ecfY}) as a function of the abundance of ECF Y proteins is shown. Here, LOW and HIGH indicate the respective protein abundances obtained at basal and maximal activity of the inducible promoter P_{ind}, which drives *ecfX* expression. (**D**) Computation model prediction of the variation of the output dynamic range of the 2-step timer circuit as a function of the circuit copy number for the two exemplary cases in which the ECF target promoter has high (dashed line) or medium (solid line) strength.

timers was in quantitative agreement with the behaviour of the 1-step timers. Here, we reasoned that if ECF σ factors would display orthogonality in different genetic environments (i.e. circuits), the dynamics of all circuits should be captured by a set of models sharing the same parameters for the same ECF σ factors. Briefly, our computational model for a 2-step timer circuit (Figure 3A) comprises transcription (at rates α_i) and translation (at rates β_i) of the two ECF σ factors *X* and *Y* as well as the *lux* reporter cassette ($i = X, Y, lux$), degradation and/or dilution of the resulting mRNA and protein species (at rates λ_i and δ_i, respectively), binding of the ECF σ factor to the RNA polymerase core (with binding constants K_{EX} and K_{EY}) as well as binding of the resulting holoenzymes to their cognate promoters (with binding constants $K_{EX\text{-}P}$ and $K_{EY\text{-}P}$). Analogous to the model for the 2-step timer depicted in Figure 3A, we developed similar models also for the 1- and 0-step timers (see Materials and Methods for details). In order to test for compatibility of this set of models with our experimental data, we followed a sequential approach: First, we fitted our model to the data of the 0-step timer (Figure 2B; *solid lines*), thereby inferring the kinetic parameters required to describe the P_{BAD} promoter as well as the luciferase reporter (see Supplementary Table S4). Then we fixed those parameters and varied only the parameters specific to the individual ECF σ factors, thereby fitting the models of the 1- and 2-step timers simultaneously to the experimental data (Figure 2C–F; *solid lines*). Notably, all experimental data is well captured by models sharing a single set of parameters, showing that ECF28 and ECF32 display invariant quantitative behavior when being integrated in the 1- and 2-step timers. This suggests that the functional properties of these ECF σ factors are independent of the complexity of the synthetic circuit they are used in, i.e. they behave indeed orthogonally. Moreover, when integrating all information into a model for the two variants of the 3-step timers described above, the computational model correctly predicts the experimentally observed increase in baseline activity without invoking any additional fit parameters. However, while the experimental data still displays a weak (∼2-fold) residual induction for both 3-step timers, the model predicts a complete loss of dynamic range, suggesting that the *in vivo* system retains subtle interactions that are not entirely captured in the computational model (Supplementary Figure S5; *solid lines*).

To illustrate the origin of the decreasing dynamic range within our mathematical model, we considered a scenario in which both ECF σ factors of the 2-step timer, referred to as ECFs X and Y, have identical expression strengths and promoter binding characteristics (Figure 3). Moreover, we chose a set of physiological parameter values (Supplementary Table S5) and assumed that the circuit is present at 50 copies/cell, reflecting the situation of a medium copy plasmid. Under these conditions already the basal activity of the inducible promoter is predicted to lead to an average

copy number of 3 ECF X molecules/cell, which, based on the high number of target promoters (50 copies), will in turn lead to the production of 25 ECF Y molecules/cell (Figure 3B; *lower panel*). This amplification of baseline activity is further exacerbated in the last step of the cascade, for which the reporter gene activity is almost 100-fold higher than the baseline activity of the inducible promoter (Figure 3B; *upper panel*). Ultimately, the fact that each ECF σ factors produces more ECF σ factors of the downstream step in the cascade will inevitably lead to full promoter saturation in downstream stages of longer ECF cascades. On the other hand, when considering a chromosomally integrated circuit present only at a low copy number (1–8 copies/cell, depending on growth conditions), our model predicts that even at full activation of the first ECF σ factor, each subsequent step in the cascade will produce less ECFs than the previous one, leading to a quick decay of circuit's maximal output with increasing cascade length (Figure 3C). Only at intermediate circuit copy numbers – when the output-dynamic range of the first ECF σ factor optimally matches the input-dynamic range of the second ECF σ factor does our model predicts an improved signal transmission through the 2-step timer circuit (Figure 3D; *solid line*). Note that the optimal circuit copy number, however, critically depends on the strength of the ECF promoters involved. For stronger promoters, our model predicts that lower circuit copy numbers are required to achieve maximal signal transmission (Figure 3D; *dashed line*). From this we expected that timer circuits comprising strong ECF target promoters would display a higher output dynamic range on single copy than on a multi-copy plasmid.

Expression dynamics and signal propagation in chromosomally integrated timer circuits

Based on our predictions, we next addressed the question if a reduction in circuit copy number would improve signal transmission in our ECF cascades. Towards that end, we integrated all 0-, 1- and 2-step timers into the chromosome of *E. coli* (see Materials and Methods for details) and monitored luciferase activity upon induction with different arabinose concentrations (Figure 4). For the 0-step timer (P_{BAD}-*lux,* Figure 4B), the maximal activity at high arabinose levels was decreased by a factor of 15 when compared to the plasmid-encoded 0-step timer (Figure 2B). Surprisingly, the basal activity decreased by a factor of ≥400 (reaching the lower luciferase detection limit), leading to an overall output-dynamic range of at least 50000x for the chromosomally integrated construct (Figure 4B). Although the molecular origin for this context-dependence remains elusive, it is plausible that the DNA loop required for P_{BAD} repression in the absence of arabinose (34) is more stable on the chromosome as compared to the medium copy plasmid, which might lead to tighter P_{BAD} regulation of the chromosomally integrated construct. Consistent with this low basal activity of P_{BAD}, we found that the basal activity of all 1- and 2-step timers also remains at the lower detection limit (Figure 4C-F), confirming our model prediction that the OFF state should be stably maintained for low copy timer circuits (Figure 3C). Likewise, our model predicted a decrease of the maximal output strength with increasing ECF cascade length, which we qualitatively confirmed in all chromosomal timer circuits (Figure 4C–F). Output reduction, however, was far stronger in the ECF28-based 1-step timer (250-fold; Figure 4C) compared to the ECF32-based 1-step timer (2.5-fold; Figure 4D), suggesting the existence of non-linear effects also in the regulation of ECF target promoters, which cannot be explained by mere circuit copy number reduction. Concomitant with output reduction we also observed an apparent increase in time delay, which was much stronger in the ECF28-based 1-step timer (130 min) compared to the ECF32-based 1-step timer (15 min) (Figure 4C and D). When combining the two ECFs into 2-step timer circuits in different permutations (Figure 4E-F), the time delay slightly increased to 140 min (Figure 4E) and 135 min (Figure 4F), while the output dynamic range only decreased to 80-fold and 50-fold, respectively. These data show that a reduction of circuit copy number indeed improves signal transmission through the 2-step timers, ending up with a more than 10-fold higher output dynamic range than for the equivalent plasmid-encoded circuits (cf. Figure 2E and F). However, integrating the circuits into the *E. coli* chromosome still lead to a decrease of maximal signal strength with increasing ECF cascade length, suggesting that in the future additional fine-tuning of ECF σ factor expression levels to match their cognate target promoter characteristics will help improving signal transmission even further.

Implementation of orthogonal ECF switches in *B. subtilis*

We next aimed at expanding the potential of ECF σ factors as synthetic orthogonal regulators beyond the *E. coli* species border. We therefore chose to implement of ECF switches in the Gram-positive model organism *B. subtilis*. We selected 10 ECF-promoter pairs (Supplementary Table S1) from organisms belonging to the *Proteobacteria*, *Actinobacteria* and *Firmicutes* (8,35), such that members of the chosen ECF groups were not present in *B. subtilis*, thereby minimizing the probability of undesired cross-reactions. Functionality of ECF σ factors in *B. subtilis* was tested by placing the ECF-encoding genes under the control of the LIKE expression system, which is based on the bacitracin-inducible P_{liaI} promoter (36). The ECF target promoters were transcriptionally fused to a *B. subtilis*-adapted luciferase cassette (24,37). As a host, we used *B. subtilis* strain 168 and integrated each TU at a different locus on the chromosome (see Supplementary Table S3), to avoid any negative effects of poor insulation of the components of the switch. All chosen loci are located close to the chromosomal origin of replication, assuring that any negative positioning effects are minimized (24,38).

Out of the 10 ECF-promoter pairs tested, we found that three ECF target promoters (ECF41, ECFUN and ECF105) displayed strong activity when their cognate ECF σ factor was expressed (Supplementary Figure S6A), while the other seven constructs did not show any discernable luciferase activity (data not shown). Here, titration of ECF41, ECFUN and ECF105 lead to a 100-, 30- and 15-fold upregulation of their cognate target promoters, respectively, while the negative control strains not expressing the ECF σ factors showed target promoter activities close to the luminescence background (Supplementary Figure S7). More-

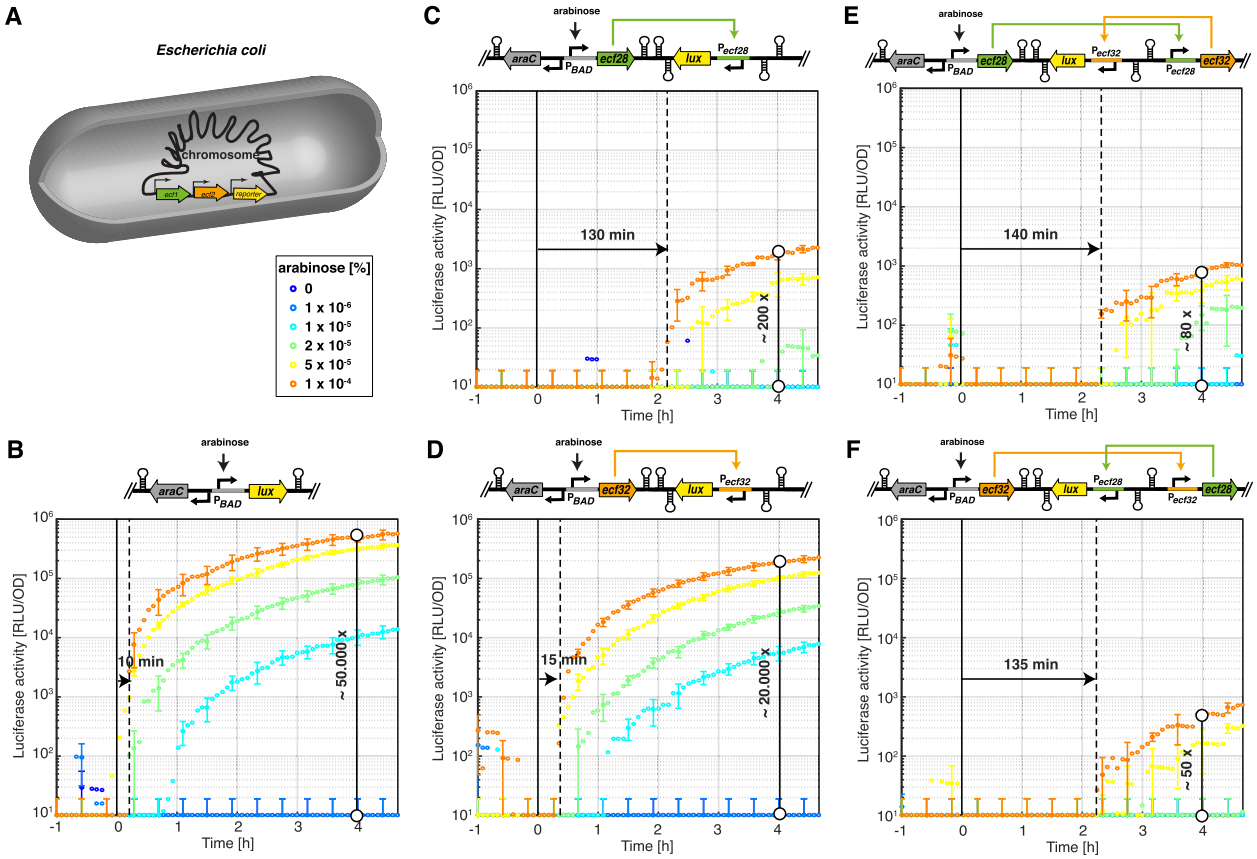

Figure 4. Single-copy autonomous timer circuits in *E. coli*. (**A**) All circuits shown in the cartoons of (**B**–**F**) were integrated into the chromosome of *E. coli* strain SV01 using the pSV plasmid series (Supplementary Table S2). Panels (B–F) show the dynamical response of luciferase activity (shown in relative luminescence units normalized by the optical density measured at 600 nm) in synthetic ECF cascades featuring no (B), one (C, D) and two (E, F) ECF σ factors, after the addition of various concentrations of arabinose at $t = 0$ h (*black solid line*). The time delay of gene induction (*black dashed line*) is indicated for the highest arabinose concentration (10^{-4}%) and was defined as the time when luciferase activity first exceeded the pre-induction value by 2-fold. Maximal fold induction is also indicated. The experimental response dynamics (*circles*) was recorded during exponential growth, as described in Materials and Methods.

over, the expression of one type of ECF σ factor did not trigger the activation of non-cognate ECF target promoters (Supplementary Figure S8C and D), showing that there is no discernable cross-regulation between these heterologous ECF switches within our experimental detection limit. While these observations demonstrate specific activation of the target promoters by their cognate ECF σ factors, we also tested whether overexpression of these ECF σ factors had any adverse effects on *B. subtilis* physiology. But neither the growth behavior in LB medium (Supplementary Figure S6B) nor the expression behavior of a housekeeping promoter (P_{lepA}, (24)) were affected by the overexpression of any of the three ECF σ factors (Supplementary Figure S6C and D). These data highlight the potential of ECF σ factors as orthogonal regulators also in the Gram-positive model organism *B. subtilis*.

Behavior of ECF cascades in *B. subtilis*

Besides implementing ECF switches in *B. subtilis*, we also wanted to probe whether ECF σ factors are amenable to higher order circuit design in this host. Towards this end we used the three functional ECF σ factors implemented above, and constructed chromosomally encoded ECF timers in *B. subtilis* (see Materials and Methods for details). When comparing the dynamic behavior of the 0-step timer (P_{liaI}-*lux*) to the one of the 1-step timers containing ECF41, ECFUN and ECF105, we found that the quick response of the 0-step timer (5 min; Figure 5B) was delayed in the 1-step timers (15–20 min; Figure 5C-D and Supplementary Figure S7C) and even more in the 2-step timers combining ECF41 and ECFUN (40 min; Figure 5E and F). These values are comparable to the doubling time of *B. subtilis* (35 min in LB medium at 30°C), in agreement with our observations in *E. coli*. Likewise, also the output-dynamic range decreased from a ∼200-fold induction in the 0-step timer to a ∼15–100-fold induction in the 1-step timers (Figure 5C and D and Supplementary Figure S7C). In *B. subtilis*, both the maximal activity as well as the baseline decreased from the 0-step to the 1-step timers. This is even more pronounced in the 2-step timers that combine ECF41 and ECFUN, for which the overall activity approaches the lower detection limit of luciferase activity, thereby reducing the induction range to 3-fold (ECF41-ECFUN-*lux;* Figure 5E) and 8-fold (ECFUN-ECF41-*lux;* Figure 5F). Note that luciferase signals close to the detection limit naturally display higher sample-to-sample variability, which leads to in-

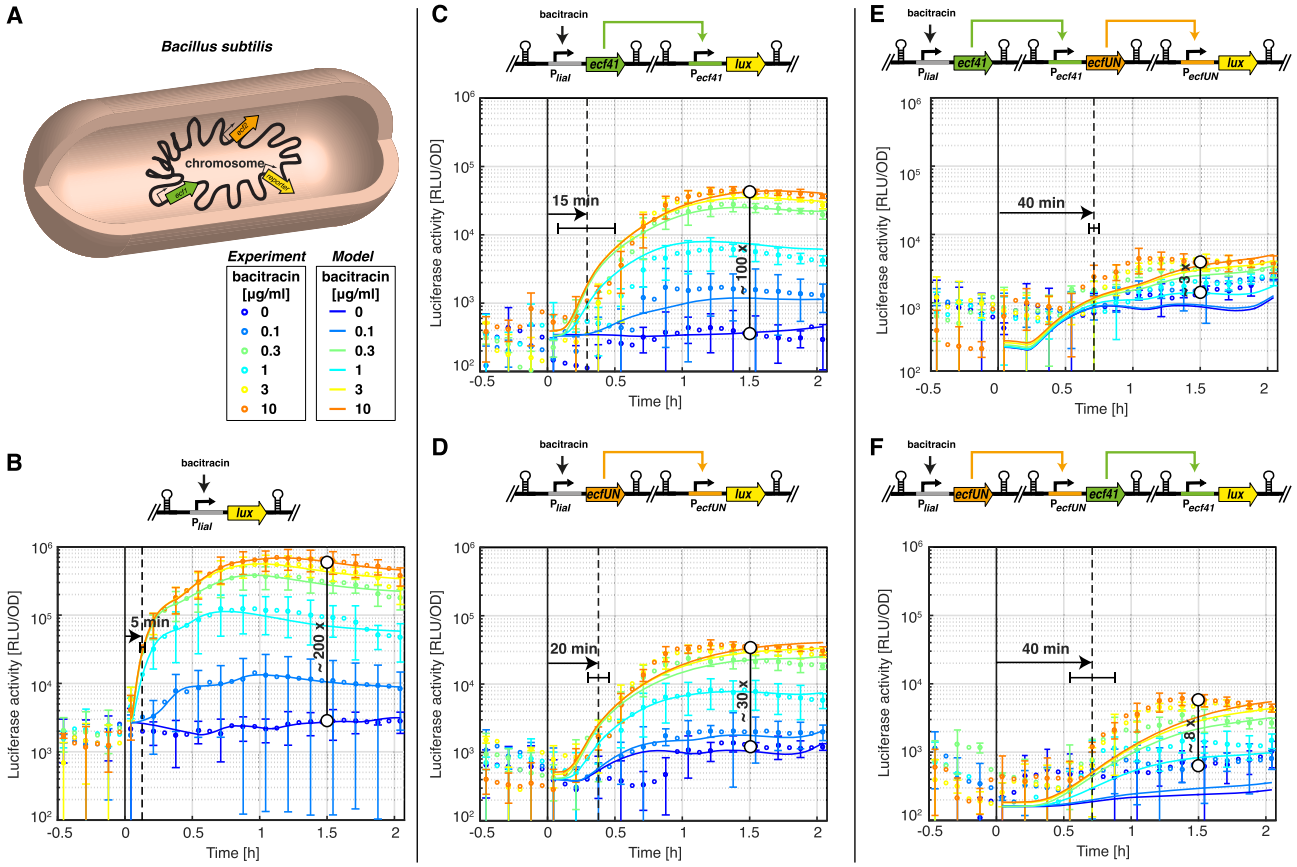

Figure 5. Time delayed response of synthetic ECF cascades in *B. subtilis*. (**A**) All circuits shown in the cartoons of (**B**–**F**) were integrated into the chromosome of *B. subtilis* 168. Panels (B–F) show the dynamical response of luciferase activity (shown in relative luminescence units normalized by the optical density measured at 600 nm) in synthetic ECF cascades featuring no (B), one (C, D) and two (E, F) ECF σ factors, after the addition of various concentrations of bacitracin at $t = 0$ h (*black solid line*). The time delay of gene induction (*black dashed line*) is indicated for the highest bacitracin concentration (10 μg/ml) and was defined as the time when luciferase activity first exceeded the pre-induction value by 2-fold. Maximal fold induction is also indicated. The experimental response dynamics (*circles*) was recorded throughout growth, as described in Materials and Methods. The response dynamics of the computational model (*solid colored lines*) was obtained by a simultaneous fit of all experimental data in (B–F), showing that the behavior of all 5 circuits can be explained with one self-consistent set of physiological parameters (see Supplementary Table S6). Here, the time delays in the computational model (as given for 10 μg/ml bacitracin) are: (B) 5 min, (C) 12 min, (D) 14 min, (E) 25 min and (F) 35 min.

creased measurement noise and hence higher standard deviations (error bars) in the *B. subtilis* data. However, overall these results are in qualitative agreement with the expectation raised by our computational model (Figure 3C), which predicted a decay of the overall signal strength with increasing length of the σ factor cascade for single-copy ECF timer circuits. This data also fits our observations on the behavior of the chromosomally encoded *E. coli* timer circuits (cf. Figure 4). Taken together, these results clearly demonstrate that more complex ECF circuits can also be functionally assembled in *B. subtilis*, where they display similar characteristics to ECF circuits in *E. coli*.

Computational model for σ factor cascades in *B. subtilis*

Based on the convergent qualitative behavior of ECF circuits in both organisms, we wondered whether the experimental data in *B. subtilis* is also quantitatively consistent with our computational model. Adapting all species-specific model parameters to those known for *B. subtilis* (Supplementary Table S6) and estimating the remaining ones in a sequential fitting approach as described above, indeed showed that the kinetic response of all circuits was well-captured with a single set of parameters (solid lines in Figure 5 and Supplementary Figure S7). During the fitting process it was necessary to incorporate time-dependent basal promoter activities of P_{ecfUN} and P_{ecf105} into the model, as they slightly increase at $t = 0.5$–1 h even in the absence of inducer (Figure 5D and Supplementary Figure S7C). Since this behavior is also found in the negative controls not expressing any heterologous ECF σ factors (Supplementary Figure S7E and F) and since it coincides with the end of exponential phase (see Supplementary Figure S11), it is conceivable that P_{ecfUN} and P_{ecf105} are partially recognized by one of the endogenous σ factors of *B. subtilis*, some of which are up-regulated during transition phase of *B. subtilis* (39,40). While these observations suggest that orthogonality of ECF switches is reduced during transition phase, we would like to emphasize that these non-specific modulations on basal ECF promoter activities are small (2–3-fold), and thus still allow for predictable circuit behavior even during the entry into stationary phase. Indeed, within

our model both the delayed response times as well as the decreasing dynamic range for longer ECF cascades was accurately captured (solid lines in Figure 5 and Supplementary Figure S7). Moreover, as was the case for *E. coli*, the model predicts an almost complete loss of output-dynamic range for the 3-step timer circuits in *B. subtilis,* which we also confirmed experimentally (see Supplementary Figure S9).

Recovery of signal transmission in *B. subtilis* chromosomally encoded ECF cascades

Our computational analysis suggested that signal transmission in ECF σ factor cascades can be improved by lowering the overall ECF σ factor expression level in plasmid-encoded circuits. But reducing the copy number (from ∼50 in plasmid-encoded circuits to ∼1 in chromosomally-encoded circuits) lead to a loss of maximal output signal, both in *E. coli* and *B. subtilis* (Figures 4 and 5). For recovering signal transmission, we increased the expression level of only the first ECF σ factor of the cascade, as it has been previously shown that such an approach can recover the loss of output imposed by the reduction in copy number on a toggle switch (41). We have used the *B. subtilis* 2-step timers as a test case and placed the first TU (P_{liaI}-ECF41 or P_{liaI}-*ECFUN*) on a multi-copy plasmid, while keeping the other two TUs (P_{ecf41}-*ECFUN* and P_{ecfUN}-*lux* or P_{ecfUN}-*ECF41* and P_{ecf41}-*lux*) on the chromosome (Supplementary Figure S10). These partially plasmid-encoded 2-step timers showed a similar time delay to their chromosomally encoded counterparts, and indeed reached higher maximal activity levels that were not accompanied by an increase of the baseline (Supplementary Figure S10). The resulting increases in dynamic range (from 3- to 6-fold in the ECF41-ECFUN-*lux* 2-step timer and from 8- to 12-fold in the ECFUN-ECF41-*lux* timer) demonstrate that the behavior of the ECF timers can be improved by fine-tuning the expression levels of its components.

Taken together, our results unveil a fundamental limitation for signal propagation via σ factor cascades, which is linked to the fact that σ factors operate in a non-cooperative manner. Indeed, σ factors bind to RNA polymerase as monomers, and so do the resulting holoenzymes to their promoters (27). Accordingly, the dose–response curves of ECF promoters are hyperbolic (with an effective Hill exponent ≤ 1), such that double the σ factor concentration can maximally lead to double the target promoter activity. Given that the dose-response curve is additionally limited by a basal promoter activity at low, and by promoter saturation at high ECF σ factor levels, a given input-dynamic range of ECF σ factor concentrations will almost certainly be transferred into a lower output-dynamic range of the downstream ECF σ factor, i.e. information will be lost within this step in the cascade. While our current design does not circumvent this limitation, our model shows that by fine-tuning the magnitude of output gene expression to match precisely the diagonal in Figure 3B–C, e.g. by adjusting the overall expression strength of the downstream ECF σ factor, it is possible to optimize signal transmission to its theoretical maximum.

Switching kinetics of ECF cascades from ON to OFF

How do the constructed timer circuits respond when the expression of the first gene in the cascade is suddenly turned OFF? Similar to the switching kinetics when suddenly turned ON, theory predicts that there should be also an increasing time delay with increasing cascade length for the reverse switching direction (Supplementary Figure S12A). This is based on the fact that after shut-down of the first promoter, ECF σ factor levels have to be diluted and/or degraded below the activation threshold for their target promoter, such that expression of the downstream σ factor is turned OFF, etc. To test this prediction experimentally we first pre-induced timer circuits in *E. coli* and *B. subtilis* with their highest inducer levels (10^{-4}% arabinose and 10 μg/ml bacitracin, respectively), then washed cells with inducer-free medium and monitored luciferase activity in a microplate reader (Figure 6). For the ECF σ factor cascades in *E. coli* (Figure 6A), we observed that after inducer removal ($t = 0$ h), luciferase activity first increased ∼2-fold within 0.5 – 2 h and then decreased with different rates. This somewhat unexpected increase in luciferase activity after inducer removal is presumably caused by a transient decrease in the growth rate after the washing step (Supplementary Figure S12B), which results in a decreased protein dilution rate and hence in increased accumulation of luciferase enzymes. Importantly, closer inspection of the switching kinetics shows that both the time at which luciferase activity peaks (Figure 6A), as well as the timescale at which the luciferase signal decays (Figure 6C) increases with the number of genes in the ECF cascade, as expected qualitatively. Here, the signal half-life time of the 0-step timer (130 min) is only slightly faster than the cell doubling time in these experiments (∼175 min), suggesting that the luciferase enzymes are mostly stable and only diluted due to cell growth. While longer ECF cascades display up to a 2–4 fold increase in signal half-life times (Figure 6C), for the 1-step timer involving ECF32 the signal half-life time is very similar to the 0-step timer. This is consistent with the fact that our model predicted low protein stability for ECF32 from the induction experiments above (cf. Supplementary Table S4). Interestingly, when simulating our computational model with the parameter set inferred before, the theoretical prediction for the switching kinetics from ON to OFF is strikingly similar to the experimental response dynamics – displaying also a growth rate-induced peak in luciferase signal (Figure 6B). Although the signal half-life time predicted by the model is slightly higher than determined experimentally (Figure 6C), the model captures the temporal hierarchy of switching kinetics across the different cascades very well – including also the rapid OFF-switching of the ECF32-containing 1-step timer (Figure 6C; *cyan bars*).

Parallel to these observations in *E. coli*, we found that when switching the ECF σ factor cascades in *B. subtilis* from ON to OFF by washing cells with inducer-free medium, they also displayed a longer signal half-life time with increasing cascade length (Figure 6D and F). In this case, we did not observe a growth-delay after the washing step, and accordingly an almost instant exponential decrease in luciferase signals until cells enter the transition to stationary phase after ∼1.5 h. Strikingly, also here the

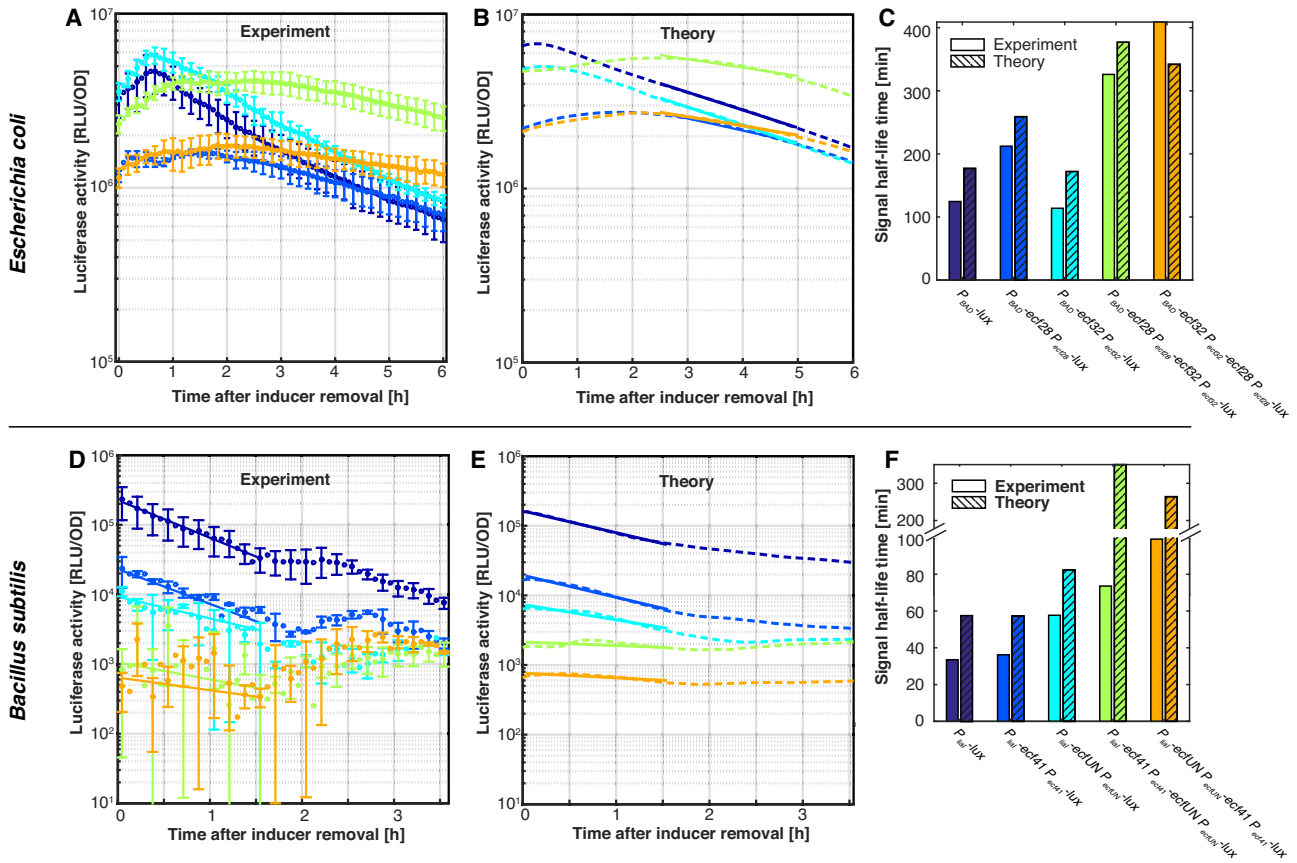

Figure 6. Switching synthetic ECF cascades from ON to OFF state. Decay of luciferase activity in (**A**) plasmid-encoded timer circuits in *E. coli* and (**D**) chromosomally integrated timer circuits in *B. subtilis*, when cells are shifted from inducer-rich (10^{-4}% arabinose in (A), 10 μg/ml bacitracin in (D)) to inducer-free medium at $t = 0$ h. The strains used in (A) and (D) are identical to those in Figures 2 and 5, respectively. Symbols and error bars indicate mean and standard deviation from three independent biological replicates. (**B**) and (**E**) show the computational prediction (*dashed lines*) for the switching kinetics from ON to OFF state in the models for the timer circuits of *E. coli* and *B. subtilis*, respectively, when the transcription rate of the inducible promoter is shifted to its basal value at $t = 0$ h. Solid lines in (A and B) correspond to fits of an exponentially decaying function, which was used to infer the experimental and theoretical signal half-life times reported in (**C** and **F**). Note that the time interval for these fits (2.5–5 h in (A and B); 0–1.5 h in (D and E)) was restricted to a period of constant exponential growth (cf. Supplementary Figure S12).

previously inferred model parameters (Supplementary Table S4) lead to model predictions that qualitatively captured the experimental kinetics (Figure 6E). This includes also the switching kinetics of the ECF41-involving 1-step timer, which displays a similarly rapid signal half-life time than the 0-step timer (Figure 6F), as predicted theoretically based on a reduced protein half-life of ECF41 (Supplementary Table S4). However, the half-life times of the 2-step timers were overestimated 2–3-fold by our model, likely because both signals are already close to the background, leading to noisy half-life estimates. In summary, these results clearly show that multi-tiered ECF σ factor cascades not only respond with a progressively longer time delay when switched ON, but also relax to their initial state more slowly when switched OFF. The striking congruence between our model predictions and the experimental dynamics further corroborates the validity of our model, and suggests that two of the heterologous ECF σ factors (ECF32 in *E. coli* and ECF41 in *B. subtilis*) are subject to proteolysis *in vivo*.

DISCUSSION

In this study we have demonstrated that heterologous ECF σ factors can be successfully implemented in two distantly related bacteria – *E. coli* and *B. subtilis* – to build orthogonal synthetic circuitry containing two or more such regulators. The ECF σ factors applied here are derived from phylogenetically distant organisms and belong to six distinct ECF subgroups. As such, they recognize different target promoter sequences and are controlled by different mechanisms (15). Despite this variation of the individual building blocks, we found a strikingly convergent circuit behavior in all assembled variants. In fact, in both organisms the ECF σ factor cascades showed the function of 'autonomous timers', with a characteristic time delay between inducer addition and activation, as well as between inducer removal and deactivation of target gene expression. The quantitative behavior of these timers can be explained by a computational model, which not only predicts the time delays imposed by the increasing length of the ECF σ factor cas-

cade, but also captures the experimentally observed loss of dynamic range in both *E. coli* and *B. subtilis*. Hence, our study demonstrates that phylogenetically different ECF σ factors share very similar functional characteristics in different model species, suggesting that ECF σ factors might be universally applicable to a range of other bacteria, including biotechnological workhorses such as *Corynebacterium glutamicum* (42) or *Pseudomonas putida* (43).

Autonomous timer circuits based on orthogonal ECF σ factors will therefore not only expand the synthetic regulatory repertoire in other important microorganisms, but also enable biotechnological applications. For instance, the yield of heterologous *myo*-inositol production in *E. coli* could be greatly enhanced by delaying the expression of engineered pathway enzymes until midway through the cultivation (44). Such a dynamic flux control allowed substrate pools to first accumulate and then be directed into the engineered pathway, analogous to the 'just-in-time transcription' frequently found in natural systems (45). While Gupta *et al.* used an engineered quorum sensing circuit to globally slave the expression of all pathway components to bacterial growth phase (44), the autonomous timers built here would allow for the introduction of a fine-tuned timing hierarchy between the expression of individual pathway components. For instance, if the ultimate product of the heterologous pathway is toxic to the cell, it is advantageous to quickly express early enzymes in the pathway and defer the expression of the last, product-forming enzyme until sufficient intermediates have accumulated, thereby maximizing total yield (46). With our ECF-based timer circuits we achieved maximal time delays of 1–2 cell doubling times in both model organisms, a timescale at which pathway intermediates could indeed accumulate. Interestingly, the time delays of our *in vivo* timer circuits are comparable to time delays measured in an *in vitro* cell free (*E. coli*) expression system (47), in which σ factor cascades generated time delays between 5 and 10 min (for a single σ factor) and 60 min (for a cascade of five σ factors).

In addition to a precise temporal control of gene expression, the optimization of biosynthetic pathway productivity critically hinges on the fine-tuning of relative enzyme stoichiometries (48). Although it would be ideal to tune expression timing and strength independently, the current prototypes of our autonomous timer circuits exhibit a strong correlation between the time delay and the overall strength of final target gene expression. Generally, our model showed that the decrease of output dynamic range in later stages of the ECF cascade can be explained with the non-cooperative regulation of ECF target promoters, resulting in an output dynamic range that will always be smaller than its input dynamic range (cf. Figure 3). Through fine-tuning the circuit copy number we showed that signal transmission through the ECF cascade can be improved (cf. Figures 4 and 6) – essentially by adjusting the output dynamic range of one ECF promoter to the input dynamic range of the next ECF promoter. Note that similar fine-tuning of input and output dynamic ranges was required when functionally connecting a library of multiple Tet repressor homologs within the genetic design environment 'Cello' (49). Likewise, during the conversion of a bistable multi-copy genetic toggle switch into a single-copy variant, bistability could only be preserved by either increasing overall expression strength or by reducing basal promoter activity (41), showing that also here the expression strength of transcriptional regulators (LacI and TetR) needs to be finely adjusted to a condition-dependent 'operating' point.

Besides fine-tuning ECF expression levels, another strategy to improve signal transmission in the timer circuits could be inspired by natural σ factor cascades, which often control complex temporal sequences of developmental processes, e.g., in the sporulation cascade of Firmicutes bacteria (50). Signal transmission in these cascades heavily relies on the expression of anti-σ factors, which can sequester σ factors into transcriptionally unproductive σ/anti-σ factor complexes. Here, sequestration reduces target promoter activity at low σ factor levels and thereby effectively causes a non-linear (ultrasensitive) dose-response behavior for rising σ levels (17,51). The introduction of heterologous anti-σ factors into synthetic timer cascades could hence facilitate signal amplification and would help generating a digital switching behavior between the OFF and ON states of the target promoter. Similarly, ultrasensitivity has been successfully exploited to build time delays in switches and cascades comprised of other regulators, such as in a synthetic DNA strand-displacement circuit (52), in a synthetic protein-protein sequestration cascade (53) or in a cascade of cooperatively regulated transcription factors (54). While these examples indicate that the introduction of ultrasensitivity via anti-σ factors could convey a number of desirable characteristics to the construction of autonomous timers and other ECF-based synthetic circuitry, it was shown that the expression of heterologous anti-σ factors is associated with significant toxicity in *E. coli* (8). This suggests that the simultaneous expression of multiple anti-σ factors will be problematic. Thus, scaling up the use of anti-σ factors in synthetic ECF circuits will only be possible if we better understand and minimize the burden incurred by anti-σ expression.

In conclusion, we have successfully implemented ECF σ factor-based autonomous timers *in vivo* and demonstrated that the concept is generally applicable to different ECF groups, organisms or genetic systems. In the future we expect that the combination of orthogonal ECF σ factors with other tools for transcriptional, translational and post-translational synthetic circuit design (55) will greatly facilitate the development of more sophisticated *in vivo* gene expression programs in a variety of biotechnological applications and production hosts.

SUPPLEMENTARY DATA

Supplementary Data are available at NAR Online.

ACKNOWLEDGEMENTS

We thank Torsten Waldminghaus and Matthew McIntosh for advice and help with the cloning strategy. D.P., S.V., T.M. and G.F. conceived the experiments, D.P. and S.V. conducted the experiments, D.P., S.V., H.W., M.M. and G.F. analysed the results, H.W., M.M. and G.F. developed the model, D.P. and G.F. wrote the manuscript.

FUNDING

LOEWE Program of the State of Hesse (SYNMIKRO); German Federal Ministry of Education and Research [031L0010A to T.M., 031L0010B to G.F.] funded in the framework of the ERASynBio initiative; People Programme (Marie Curie Actions) of the European Union's Seventh Framework Programme [628509 to D.P.]. Funding for open access charge: Bundesministerium für Bildung und Forschung [031L0010B].

Conflict of interest statement. None declared.

REFERENCES

1. Guet,C., Elowitz,M.B., Hsing,W. and Leibler,S. (2002) Combinatorial synthesis of genetic networks. *Science*, **296**, 1466–1470.
2. Morey,K.J., Antunes,M.S., Barrow,M.J., Solorzano,F.A., Havens,K.L., Smith,J.J. and Medford,J. (2012) Crosstalk between endogenous and synthetic components–synthetic signaling meets endogenous components. *Biotechnol. J.*, **7**, 846–855.
3. Del Vecchio,D. (2015) Modularity, context-dependence, and insulation in engineered biological circuits. *Trends Biotechnol.*, **33**, 111–119.
4. Gao,Y., Xiong,X., Wong,S., Charles,E.J., Lim,W.A. and Qi,L.S. (2016) Complex transcriptional modulation with orthogonal and inducible dCas9 regulators. *Nat. Methods*, **13**, 1043–1049.
5. Chappell,J., Takahashi,M.K. and Lucks,J.B. (2015) Creating small transcription activating RNAs. *Nat. Chem. Biol.*, **11**, 214–220.
6. Westbrook,A.M. and Lucks,J.B. (2017) Achieving large dynamic range control of gene expression with a compact RNA transcription-translation regulator. *Nucleic. Acids. Res.*, **45**, 5614–5624.
7. Stanton,B.C., Nielsen,A.A.K., Tamsir,A., Clancy,K., Peterson,T. and Voigt,C.A. (2014) Genomic mining of prokaryotic repressors for orthogonal logic gates. *Nat. Chem. Biol.*, **10**, 99–105.
8. Rhodius,V.A., Segall-Shapiro,T.H., Sharon,B.D., Ghodasara,A., Orlova,E., Tabakh,H., Burkhardt,D.H., Clancy,K., Peterson,T.C., Gross,C.A. *et al.* (2013) Design of orthogonal genetic switches based on a crosstalk map of σs, anti-σs, and promoters. *Mol. Syst. Biol.*, **9**, 1–13.
9. Mueller-Hill,B. (1996) *The Lac Operon: A Short History of a Genetic Paradigm*. Walter de Gruyter, Berlin.
10. Bertram,R. and Hillen,W. (2008) The application of Tet repressor in prokaryotic gene regulation and expression. *Microb. Biotechnol.*, **1**, 2–16.
11. Schleif,R. (2010) AraC protein, regulation of the l-arabinose operon in *Escherichia coli*, and the light switch mechanism of AraC action. *FEMS Microbiol. Rev.*, **34**, 779–796.
12. Staroń,A., Sofia,H.J., Dietrich,S., Ulrich,L.E., Liesegang,H. and Mascher,T. (2009) The third pillar of bacterial signal transduction: classification of the extracytoplasmic function (ECF) sigma factor protein family. *Mol. Microbiol.*, **74**, 557–581.
13. Jogler,C., Waldmann,J., Huang,X., Jogler,M., Gloeckner,F.O., Mascher,T. and Kolter,R. (2012) Identification of proteins likely to be involved in morphogenesis, cell division, and signal transduction in Planctomycetes by comparative genomics. *J. Bacteriol.*, **194**, 6419–6430.
14. Huang,X., Pinto,D., Fritz,G. and Mascher,T. (2015) Environmental sensing in Actinobacteria: a comprehensive survey on the signaling capacity of this phylum. *J. Bacteriol.*, **197**, 2517–2535.
15. Pinto,D. and Mascher,T. (2016) *The ECF Classification: A Phylogenetic Reflection of the Regulatory Diversity in the Extracytoplasmic Function σ Factor Protein Family*. John Wiley & Sons, Inc., Hoboken.
16. Zong,Y., Zhang,H.M., Lyu,C., Ji,X., Hou,J., Guo,X., Ouyang,Q. and Lou,C. (2017) Insulated transcriptional elements enable precise design of genetic circuits. *Nat. Commun.*, **8**, 52.
17. Chen,D. and Arkin,A.P. (2012) Sequestration-based bistability enables tuning of the switching boundaries and design of a latch. *Mol. Syst. Biol.*, **8**, 620.
18. Ferrell,J.E. and Ha,S.H. (2014) Ultrasensitivity part III: cascades, bistable switches, and oscillators. *Trends Biochem. Sci.*, **39**, 612–618.
19. Weber,E., Engler,C., Gruetzner,R., Werner,S. and Marillonnet,S. (2011) A modular cloning system for standardized assembly of multigene constructs. *PLoS One*, **6**, e16765.
20. Kogenaru,M. and Tans,S.J. (2014) An improved *Escherichia coli* strain to host gene regulatory networks involving both the AraC and LacI inducible transcription factors. *J. Biol. Eng.*, **8**, 1–5.
21. Marx,C.J. and Lidstrom,M.E. (2002) Broad-host-range cre-lox system for antibiotic marker recycling in gram-negative bacteria. *BioTechniques*, **33**, 1062–1067.
22. Haldimann,A. and Wanner,B.L. (2001) Conditional-replication, integration, excision, and retrieval plasmid-host systems for gene structure-function studies of bacteria. *J. Bacteriol.*, **183**, 6384–6393.
23. Harwood,C.R. and Cutting,S.M. (1990) *Molecular Biological Methods for Bacillus*. John Wiley and Sons Ltd, Chichester.
24. Radeck,J., Kraft,K., Bartels,J., Cikovic,T., Dürr,F., Emenegger,J., Kelterborn,S., Sauer,C., Fritz,G., Gebhard,S. *et al.* (2013) The *Bacillus* BioBrick Box: generation and evaluation of essential genetic building blocks for standardized work with *Bacillus subtilis*. *J. Biol. Eng.*, **7**, 29.
25. UniProt Consortium (2015) UniProt: a hub for protein information. *Nucleic Acids Res.*, **43**, D204–D212.
26. Rosenfeld,N. and Alon,U. (2003) Response delays and the structure of transcription networks. *J. Mol. Biol.*, **329**, 645–654.
27. Hansen,U.M. and McClure,W.R. (1980) Role of the sigma subunit of *Escherichia coli* RNA polymerase in initiation. I. Characterization of core enzyme open complexes. *J. Biol. Chem.*, **255**, 9556–9563.
28. Chock,P.B. and Stadtman,E.R. (1977) Superiority of interconvertible enzyme cascades in metabolic regulation - Analysis of monocyclic systems. *Proc. Natl. Acad. Sci. U.S.A.*, **74**, 2761–2765.
29. Bradley,R.W., Buck,M. and Wang,B. (2016) Tools and principles for microbial gene circuit engineering. *J. Mol. Biol.*, **428**, 862–888.
30. Chen,Y.-J., Liu,P., Nielsen,A.A.K., Brophy,J.A.N., Clancy,K., Peterson,T. and Voigt,C.A. (2013) Characterization of 582 natural and synthetic terminators and quantification of their design constraints. *Nat. Methods*, **10**, 659–664.
31. Gödeke,J., Heun,M., Bubendorfer,S., Paul,K. and Thormann,K.M. (2011) Roles of two *Shewanella oneidensis* MR-1 extracellular endonucleases. *Appl. Environ. Microbiol.*, **77**, 5342–5351.
32. Hakkila,K., Maksimow,M., Karp,M. and Virta,M. (2002) Reporter genes *lucFF*, *luxCDABE*, *gfp*, and *dsred* have different characteristics in whole-cell bacterial sensors. *Anal. Biochem.*, **301**, 235–242.
33. Fritz,G., Megerle,J.A., Westermayer,S.A., Brick,D., Heermann,R., Jung,K., Rädler,J.O. and Gerland,U. (2014) Single cell kinetics of phenotypic switching in the arabinose utilization system of *E. coli*. *PLoS One*, **9**, e89532.
34. Schleif,R. (2000) Regulation of the L-arabinose operon of *Escherichia coli*. *Trends Genet.*, **16**, 559–565.
35. Wecke,T., Halang,P., Staroń,A., Dufour,Y.S., Donohue,T.J. and Mascher,T. (2012) Extracytoplasmic function σ factors of the widely distributed group ECF41 contain a fused regulatory domain. *Microbiologyopen*, **1**, 194–213.
36. Toymentseva,A.A., Schrecke,K., Sharipova,M.R. and Mascher,T. (2012) The LIKE system, a novel protein expression toolbox for *Bacillus subtilis* based on the *liaI* promoter. *Microb. Cell Fact.*, **11**, 143.
37. Schmalisch,M., Maiques,E., Nikolov,L., Camp,A.H., Chevreux,B., Muffler,A., Rodriguez,S., Perkins,J. and Losick,R. (2010) Small genes under sporulation control in the *Bacillus subtilis* genome. *J. Bacteriol.*, **192**, 5402–5412.
38. Sauer,C., Syvertsson,S., Bohorquez,L.C., Cruz,R., Harwood,C.R., van Rij,T. and Hamoen,L.W. (2016) Effect of genome position on heterologous gene expression in *Bacillus subtilis*: An unbiased analysis. *ACS Synth. Biol.*, **5**, 942–947.
39. Hecker,M., Pane-Farre,J. and Voelker,U. (2007) SigB-dependent general stress response in *Bacillus subtilis* and related gram-positive bacteria. *Annu. Rev. Microbiol.*, **61**, 215–236.
40. Osterberg,S., del Peso-Santos,T. and Shingler,V. (2011) Regulation of alternative sigma factor use. *Annu. Rev. Microbiol.*, **65**, 37–55.
41. Lee,J.W., Gyorgy,A., Cameron,D.E., Pyenson,N., Choi,K.R., Way,J.C., Silver,P.A., Del Vecchio,D. and Collins,J.J. (2016) Creating single-copy genetic circuits. *Mol. Cell*, **63**, 329–336.
42. Unthan,S., Baumgart,M., Radek,A., Herbst,M., Siebert,D., Brühl,N., Bartsch,A., Bott,M., Wiechert,W., Marin,K. *et al.* (2015) Chassis organism from *Corynebacterium glutamicum* – a top-down

approach to identify and delete irrelevant gene clusters. *Biotechnol. J.*, **10**, 290–301.
43. Nikel,P.I., Martínez-García,E. and de Lorenzo,V. (2014) Biotechnological domestication of pseudomonads using synthetic biology. *Nat. Rev. Microbiol.*, **12**, 368–379.
44. Gupta,A., Reizman,I.M.B., Reisch,C.R. and Prather,K.L.J. (2017) Dynamic regulation of metabolic flux in engineered bacteria using a pathway-independent quorum-sensing circuit. *Nat. Biotech.*, **35**, 273–279.
45. Zaslaver,A., Mayo,A.E., Rosenberg,R., Bashkin,P., Sberro,H., Tsalyuk,M., Surette,M.G. and Alon,U. (2004) Just-in-time transcription program in metabolic pathways. *Nat. Genet.*, **36**, 486–491.
46. Weber,W., Stelling,J., Rimann,M., Keller,B., Daoud-El Baba,M., Weber,C.C., Aubel,D. and Fussenegger,M. (2007) A synthetic time-delay circuit in mammalian cells and mice. *Proc. Natl. Acad. Sci. U.S.A.*, **104**, 2643–2648.
47. Shin,J. and Noireaux,V. (2012) An *E. coli* cell-free expression toolbox: application to synthetic gene circuits and artificial cells. *ACS Synth. Biol.*, **1**, 29–41.
48. Chubukov,V., Mukhopadhyay,A., Petzold,C.J., Keasling,J.D. and Martín,H.G. (2016) Synthetic and systems biology for microbial production of commodity chemicals. *NPJ Syst. Biol. Appl.*, **2**, 16009.
49. Nielsen,A.A.K., Der,B.S., Shin,J., Vaidyanathan,P., Paralanov,V., Strychalski,E.A., Ross,D., Densmore,D. and Voigt,C.A. (2016) Genetic circuit design automation. *Science*, **352**, aac7341.
50. Fimlaid,K.A. and Shen,A. (2015) Diverse mechanisms regulate sporulation sigma factor activity in the Firmicutes. *Curr. Opin. Microbiol.*, **24**, 88–95.
51. Buchler,N.E. and Cross,F.R. (2009) Protein sequestration generates a flexible ultrasensitive response in a genetic network. *Mol. Syst. Biol.*, **5**, 272.
52. Fern,J., Scalise,D., Cangialosi,A., Howie,D., Potters,L. and Schulman,R. (2017) DNA strand-displacement timer circuits. *ACS Synth. Biol.*, **6**, 190–193.
53. Shopera,T., Henson,W.R. and Moon,T.S. (2017) Dynamics of sequestration-based gene regulatory cascades. *Nucleic Acids Res.*, **45**, 7515–7526.
54. Hooshangi,S., Thiberge,S. and Weiss,R. (2005) Ultrasensitivity and noise propagation in a synthetic transcriptional cascade. *Proc. Natl. Acad. Sci. U.S.A.*, **102**, 3581–3586.
55. Bittihn,P., Din,M.O., Tsimring,L.S. and Hasty,J. (2018) Rational engineering of synthetic microbial systems: from single cells to consortia. *Curr. Opin. Microbiol.*, **45**, 92–99.
56. Feklistov,A., Sharon,B.D., Darst,S.A. and Gross,C.A. (2014) Bacterial sigma factors: a historical, structural, and genomic perspective. *Annu. Rev. Microbiol.*, **68**, 357–376.